Click Here for Full Article

Mudslide-caused ecosystem degradation following Wenchuan earthquake 2008

Diandong Ren,[1] Jiahu Wang,[2,3] Rong Fu,[1] David J. Karoly,[4] Yang Hong,[3] Lance M. Leslie,[5] Congbin Fu,[6] and Gang Huang[6]

[1] We have applied a scalable and extensible geo-fluid model (SEGMENT) that considers soil mechanics, vegetation transpiration and root mechanical reinforcement, and hydrological processes to simulate two dimensional maps of the landslides occurrence following the 2008 Wenchuan earthquake. Modeled locations and areas generally agree with observations. The model suggests that the potential energy of earth was lowered by 1.52×10^{15} J by these landslides. With this, the vegetation destroyed transfer $\sim$235 Tg C to the dead respiring pool and transforms 5.54×10^{-2} Tg N into unavailable sediments pools and the atmosphere. The cumulative CO_2 release to the atmosphere over the coming decades is comparable to that caused by hurricane Katrina 2005 ($\sim$105 Tg) and equivalent to $\sim$2% of current annual carbon emissions from global fossil fuel combustion. The nitrogen loss is twice as much as that released by the 2007 California Fire ($\sim 2.5 \times 10^{-2}$ Tg). A significant proportion of the nitrogen loss (14%) is in the form of nitrous oxide, which can affect the atmospheric ozone layer. **Citation:** Ren, D., J. Wang, R. Fu, D. J. Karoly, Y. Hong, L. M. Leslie, C. Fu, and G. Huang (2009), Mudslide-caused ecosystem degradation following Wenchuan earthquake 2008, *Geophys. Res. Lett.*, *36*, L05401, doi:10.1029/2008GL036702.

1. Introduction

[2] An undisturbed closed terrestrial ecosystem is a slow carbon and nitrogen sink. Increased disturbance (e.g., fires, floods, and wind-throw) frequency and strength can diminish the terrestrial carbon sink [*Intergovernmental Panel on Climate Change* (*IPCC*), 2007] or may even make it a net source [*Chambers et al.*, 2007]. Landslides are an important factor for desertification over mountainous regions because they are an effective way of transferring biomass from live to dead respiring pools. It takes decades for forest stands to fully recover, and takes even longer time for the recovery of soil nutrients, especially true for rainy mountainous areas. The recent earthquake that occurred on May 12, 2008 in

Wenchuan, China, caused over $120 billion in damages to infrastructure and human fatalities. In addition to the direct destruction and devastation wrought by the earthquake itself, the ensuing mudslides are responsible for the horrifying aftermath scenes. Being able to predict the locations and timing of these mudslides, especially using numerical models with sufficient lead time is a scientifically challenging problem, but extremely important to mitigate the landslide impact.

[3] Soil nutrients available for vegetation reside in the top few meters, collocated with those affected by mudslides. Landslides cause topsoil loss in the scar region and accumulate extra soil on the alluvial fans, causing serious damage to above ground vegetation for both areas. The scar area loses nutrients that require decades to recover. The ecosystem experiences a net nutrient loss because the deposit area does not benefit from the nutrients transferred from the scar area, if the soil was originally thick enough to support vegetation growth. Mudslide-caused degradation to ecosystems is being addressed in current research, mainly because the accuracy of current mudslide models is low. Our work is intended to enhance this research area by investigating landslides during and storm-triggered mudslides after the earthquake and their damages to ecosystems. Specifically, our model simulates locations, timing, and soil movement of the landslides. We then estimate the associated soil nutrient loss, and quantify Wenchuan earthquake's carbon and nitrogen impact on mountain ecosystems using a synthetic approach combining remote sensing precipitation, field investigations of topographical features, and dynamic models for regional scale.

2. Model and Data

[4] We applied an advanced modeling tool—a scalable and extensible geo-fluid model—that explicitly accounts for soil mechanics, vegetation transpiration and root mechanical reinforcement, and relevant hydrological processes. The model considers non-local dynamic balance of the three dimensional topography, soil thickness profile, basal conditions, and vegetation coverage [*Ren et al.*, 2008] in determining the prognostic fields of the driving and resistive forces, and describes the flow fields and the dynamic evolution of thickness profiles of the medium considered, be it granular or plastic.

[5] To understand changes in mudslide frequency, geographical distribution and magnitude, the biggest concern is changes in precipitation amount and intensity, and how much either is infiltrated into the soil or is runoff. This requires a well-tailored land surface scheme that properly balances computational load and accuracy requirements.

[1]Department of Geological Sciences, Jackson School of Geosciences, University of Texas at Austin, Austin, Texas, USA.
[2]State Key Laboratory of Hydrology-Water Resources and Hydraulic Engineering, Hohai University, Nanjing, China.
[3]School of Civil Engineering and Environmental Sciences, University of Oklahoma, Norman, Oklahoma, USA.
[4]School of Earth Sciences, University of Melbourne, Melbourne, Victoria, Australia.
[5]School of Meteorology, University of Oklahoma, Norman, Oklahoma, USA.
[6]Institute of Atmospheric Physics, Chinese Academy of Sciences, Beijing, China.
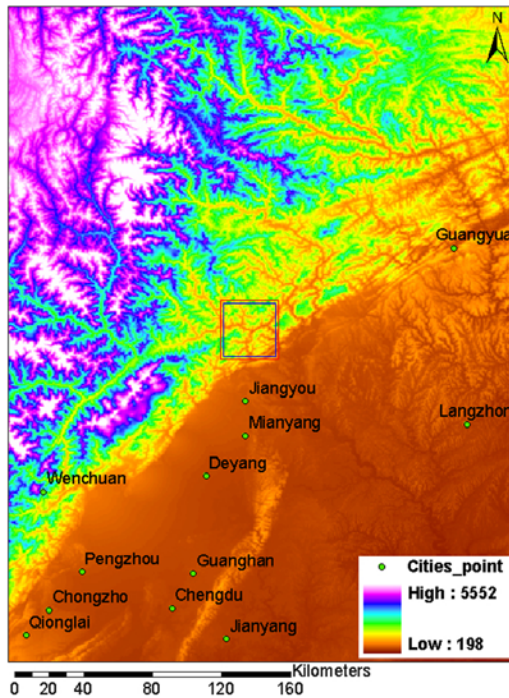
Figure 1. Digital elevation map of the southwestern China ($32.5 \sim 35.5°$N; $103 \sim 106°$E). The inset on the lower right is elevation scales. Green dots label the major cities in the vicinity. The red box is the region we display for landslide features in the following discussions.

Mudslides, especially fast-moving ones, require integration time steps on the order of 10^{-4} seconds [*Ren et al.*, 2008]. Landslides occur on spatial scales much smaller than the slopes they reside, and we need to use the finest possible digital elevation model (DEM) and soil profile data. High-resolution simulations, even for a regional area the size of a Chinese county, require in-memory processing of several Gbytes. Thus, to make the extended integration achievable in reasonable wall-clock time, simplifications of the land surface components are necessary. A force-restore scheme [*Ren and Xue*, 2004] is used instead of the resource consuming implicit solver for soil temperature. We use also the most economical approximation for evapotranspiration. The hydraulic-lift [*Ren et al.*, 2004] is not employed, based on the same consideration. Having simplified the physics, we also use only five vertical soil layers for soil moisture simulation and drainage generation.

[6] For vegetated surfaces, especially those affected by earthquake, representing soils as pure mineral soils is inadequate. Thus, we introduce organic matter content in our land surface model as provided by the Carnegie Ames Stanford Approach (CASA) [*Potter et al.*, 1993] biosphere model with improved soil moisture simulation [*Ren et al.*, 2007]. The thermal and hydraulic parameters for organic soil are obtained by weighted average of the corresponding mineral soil and those of humus, using an empirical relationship as described by *Lawrence and Slater* [2008].

[7] Where and when landslides would occur depends on local surface relief, vegetation, precipitation climatology, and seismic activity. Our study region (Figure 1) consists of several low mountain ranges located in the southwestern

China in the vicinity of Wenchuan county, the epicentre. The land cover and land use are naturally complex and comprise a mix of urban, shrub, and forest. For pre-quake conditions, we use the most recent high-resolution DEM provided by the NASA Shuttle Radar Topography Mission (SRTM, http://www2.jpl.nasa.gov/srtm/) to estimate slope and orientation of a grid cell. These data, together with the digital maps of soil characteristics prepared by the 5-min. *Global Soil Data Task* [2000] comprise the static input for our dynamic model. We also use the University of Maryland's 1 km global land cover [*Hansen et al.*, 2000] to characterize pre-quake vegetation distribution. The morphological characteristics of the root system (e.g., root distribution with depth, root distribution over different diameter classes and root area ratio), root tensile strength and tensile modulus values are assigned according to land cover type and a remote sensing retrieved above-ground biomass density map [*Zhang and Kondragunta*, 2006].

[8] In mountainous areas, besides the soil moisture condition, surface soil availability sets another limitation on saturated slab thickness [*Casadei et al.*, 2003]. We apply the following rules in initializing the sliding mass thickness. If DEM indicates that the slope is steeper than the dry material repose angle, maximum soil thickness is simply set to zero. Maximum soil thickness also is set as zero initially for impermeable surfaces (e.g., parking lots and pavements) and open waters. However, as simulation proceeds, soil slab thickness can become positive for the impermeable surfaces due to the advection from neighbouring grids.

[9] Most important for shallow landslides modeling in coarse colluviums is that root strength (>300 kPa for most chaparral shrubs) dominates the cohesion (normally less than 0.1 kPa) Following *Gray and Barker* [2004], we carefully created a mask of root strength and group distribution vertical profile according to the land cover type and the aboveground biomass. The tree root is assumed straight downward, instead of perpendicular to the local slope surface. Our parameterization of the root mechanical reinforcing of the soil shear strength achieves the following general effects: For roots of similar strength, a large number of small roots contributes most to soil reinforcement than a small number of thick roots; trees and shrubs reinforce the soil to greater depth than grasses; In addition, we consider that roots within clayey soils provide larger reinforcement than those residing in sandy soils; and that this reinforcement effect decreases exponentially with increasing soil moisture contents.

[10] May is wet season for Wenchuan region, due to the frequent passing of Plateau vortices [*Ye and Gao*, 1979]. Heavy rainfall during May 2nd and May 8th, 2008 already soaked the slopes before the initial shock. The major precipitation events on May 13th, 17th, 20th and 25th all caused significant mudslides. All precipitation data for the period May 1–31 used for driving the mudslide model were derived from the 3-hourly Tropical Rainfall Measuring Mission (TRMM) Multi-satellite Precipitation Analysis [*Huffman et al.*, 2007].

3. Results

[11] Figures 2a, 2b, and 2c are model-derived maps of surface elevation changes for May 30th 2008. Because
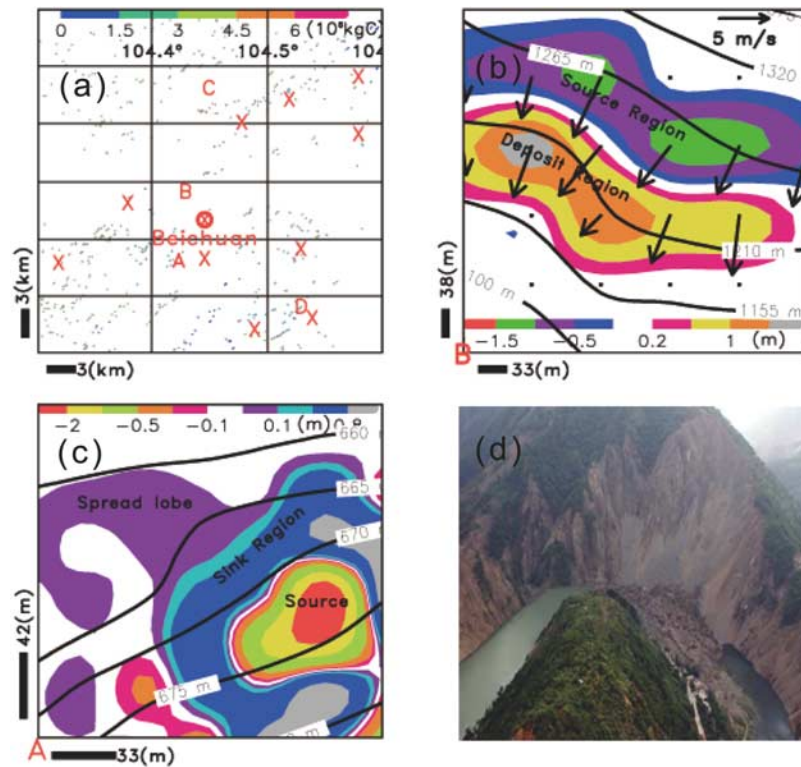
Figure 2. Landslides patterns in the interested region (red box in Figure 1). (a) Living carbon scars left by mudslides, which indicates the geographical locations of the landslides for this region. Points A, C and D label regions with conditions either in favour or preventative of landslides. Remote sensing observed landslides are labeled with cross marks, according to http://cegrp.cga.harvard.edu/category/format/gis-data/remote-sensing-image. (b) A characteristic scar formation during earthquake caused landslides (a zoomed-in look of point B in Figure 2a). After the May 12, 2008 earthquake, a ravine near Beichuan (31051′N; 104023′E) changed its surface elevation (shaded). Contour lines and the velocity field at 10 minutes after sliding set in (arrows) are also shown. The mass shed from this scar contributed to the formation of the Tangjiashan quake lake. (c) A zoomed-in look of point A in Figure 2a. (d) An aerial photo taken on May 26, 2008, showing the landslide mud that formed the Tangjiashan quake lake (Source: Xinhua news agency). In Figures 2b and 2c, the well-sorted lobe surrounding the mud source follows closely the contour lines of the pre-earthquake terrain. Figures 2b and 2d correspond to the same point B in Figure 2a.

dimensions of landslides are usually too small compared with the slopes they reside, we display only a subdomain (31.7–32°N; 104.3–104.6°E, the red box in Figure 1) of the simulation so one can see the landslide locations as highlighted speckles (Figure 2a). The most affected area is to the south of Beichuan, especially the section south of the Jian River. Although elevation is not high, the area along the zigzag section of the Jian River (marked by B at 31.83N; 104.45E) is prone to slides, due to the fact that the lateral stress of the ravines is weak and unable to effectively stop the initial basal sliding caused by the earthquake's surface wave and the fact that it is on a soft base material (X. Li, personal communication, 2008).

[12] Figure 2b shows the surface elevation change of a sliding slope marked by B in Figure 2a, superimposed by the bed elevation contours and the velocity field 10 minutes after the flow onset. The earthquake contributed most to the slip and the formation of this scar because the material resides originally on a slope gentler than the repose angle for the then soil moisture condition. A quake surface wave triggered basal sliding that initiated the movement through liquefying the top ∼2 m slab. The sliding materials are not spread-out widely (the aspect ratio, defined by the down-gradient direction length of the lobe and the parallel-elevation contour direction width, is close to unity). The material reaches a maximum speed of 5 m s^{-1} but only briefly because the resistance stress is strong for the still coherent sliding material. The complete cycle of the sliding is reasonably delineated. Lack of high resolution geodetic data prevents a direct verification of these subtle landslide features. Fortunately, a picture of this scar is available (Figure 2d) and the shape and area (∼0.2 km^2) both are close to our model estimation. We compared media reported landslide images (located at cross marks in Figure 2a) with our model predictions. Although there are errors in magnitude and exact location of the pattern, but the visual correspondence is remarkable, given the complex distribution associated with details in topography and local geology.

[13] Figure 2c provides an example of precipitation-triggered mudslide (a mesa near point 'A' on Figure 2a) with a wider-spreading tongue. The micro features of mud source region and a spreading, well-sorted lobe are clearly identifiable. Analysis of model results indicates that precipitation triggered mudslides are generally of smaller magnitudes, have a larger mud-spread lobe, and a larger aspect ratio. Zoomed-in look through the entire area indicates that

the locales of mudslides are often along the rivers, at the junctions of ravine with canyons, near the upper points of alluvial fans, or the foot of a steep slope. These agree with many previous studies [*Campbell*, 1975; *Keefer et al.*, 1987; *Iverson*, 2000; *Godt et al.*, 2006]. Although soil slips tend to form on steep slopes, there is an exception in this region. Most areas of the Tangjiashan mountain ranges (region C in Figure 2a) are not prone to mudslide because, although the slopes are steep, the soils are very shallow or nonexistent. They are underlain by an un-fractured granite rock base, which further reduces the possibility of rain-triggered mudslides. The situation for region D is just the opposite: gentler slopes, lower elevations, but thicker soils. Significant mudslides occurred in region D. This confirms the importance of saturated soil thickness in controlling the magnitude of slides (T. van Asch, personal communication, 2008).

[14] A small, fast-moving landslide in a high-population-density area may pose a greater threat to public safety than a large, slow-moving landslide. This suggests that the mud traveling velocity is likely the single most important index for measuring destructibility. We stipulate a modification to surface elevation larger than 1.5 m and a maximum attainable sliding speed larger than 1.0 m s^{-1} as the criteria for vegetation mortality and burial. Different vegetations and their different parts have quite different C/N ratios. For our domain, improved CASA yields a 420–500 gC and a 6–10 gN per kilogram of buried total biomass. Our estimation of the carbon transfer from live to dead respiring pool is ∼235 Tg, larger than the living carbon loss caused by Hurricane Katrina (∼105 Tg) [*Chambers et al.*, 2007], and amounts approximately 2% of current global annual carbon emissions by fossil fuel combustion [*IPCC*, 2007].

[15] The dead biomass pool is unable to effectively retain nitrogen. Mudslides create a favorable litter quality and quantity, soil moisture, and temperature condition for a promoted net nitrogen mineralization and create a larger nitrate gradient between the aerobic layer and the underlain anaerobic layer, where it is denitrified into gaseous state and lost to the atmosphere. Considering the precipitation climatology over the interested region, the nitrogen recovery rate by the succession species is less than 10%. Mudslides are estimated to cause gaseous loss of 5.54×10^{-2} Tg available nitrogen. The CASA model output indicates that a significant proportion of the nitrogen loss (14%) is in the form of nitrous oxide. Figure 2a is the geographical distribution patterns of the long-term (>15 years) nitrogen loss after possible vegetation recovery. Having more fertile soils, mudslides that occurred near Guangyuan to the east and Jiangyou to the south all have more severe nitrogen loss than that shown in Figure 2a. Although the absolute amount is two orders of magnitude smaller than the carbon loss, loss of nitrogen is responsible for a disproportionately large part of the mudslide-related ecosystem damage.

[16] Using the geologic map for the interested region and comparing surface elevation changes before and after the landslides, the model suggests that the potential energy of earth was lowered by 1.52×10^{15} J. Using the high-resolution land use mask, our model also outputs the total soil mass that spreads to urbanized area, how much area it covers, and the total amount of soil loss to open waters. For the region of interest, $\sim 1.18 \times 10^{8}$ m^3 of mud were shed on infrastructures, covering an area of about 110 km^2. The quake-caused extra loss of mud is about 64% of the total mass loss during the month-long period. Soil loss to the open waters is minuscule compared with the new granular material created by the quake. Except for those caused directly by the earthquake, mudslides do not occur simultaneously, due primarily to the heterogeneity of rainfall precipitation and its temporal morphology. Most of the mudslides occur after May 13th, as a result of an unfortunate combination of a major storm event and the initial shock that created plenty of granular material covering unstable slopes.

[17] Compared with fires (e.g., the southern California Fires 2007, which emitted $\sim 2.5 \times 10^{-2}$ TgN in just one-week, (C. Wiedinmyer, personal communication, 2007)) and hurricane inundation, landslides caused deforestation is unique in that they involve highly biased nutrient redistribution. Limited soil nutrient and moisture supply make the subsequent vegetation recovery more difficult for the scars. In addition, the scar regions tend to be mid-slopes, causing abrupt reduction in shearing resistance for the upstream slab. This makes future slides easier when triggering factors are ready. Earthquakes are an infrequent natural disturbance. However, by breaking down the shearing resistance between the soil/rock particles in the Qinling hills, the Wenchuan earthquake liquefied many slopes and made them vulnerable to storm-triggered mudslides. This study considers only the primary landslides following the quake. Significant parts of the study area is 'conditionally unstable-stable only when being not-so-wet' and we anticipate future slope movements in the following rainy seasons to come.

References

Campbell, R. (1975), Soil slips, debris flows and rainstorms in the Santa Monica Mountains and vicinity, southern California, *U.S. Geol. Surv. Prof. Pap., 851*.

Casadei, M., W. Dietrich, and N. Miller (2003), Testing a model for predicting the timing and location of shallow landslide initiation in soil-mantled landscapes, *Earth Surf. Processes Landforms, 28*, 925–950.

Chambers, J., J. Fisher, H. Zeng, E. Chapman, D. Baker, and G. Hurtt (2007), Hurricane Katrina's carbon footprint on U.S. Gulf Coast forests, *Science, 318*, 1107.

Global Soil Data Task (2000), *Global Soil Data Products* [CD-ROM], Oak Ridge Natl. Lab., Oak Ridge, Tenn.

Godt, J., R. Baum, and A. Chleborad (2006), Rainfall characteristics for shallow land-sliding in Seattle, Washington, USA, *Earth Surf. Processes Landforms, 31*, 97–110.

Gray, D., and D. Barker (2004), Root-soil mechanics and interactions, in *Riparian Vegetation and Fluvial Geomorphology, Water Sci. Appl.*, vol. 8, edited by J. J. Bennett and A. Simon, pp. 113–123, AGU, Washington, D. C.

Hansen, M. C., R. DeFries, J. Townshend, and R. Sohlberg (2000), Global land cover classification at 1km resolution using a classification tree approach, *Int. J. Remote Sens., 21*, 1331–1364.

Huffman, G., R. Adler, D. Bolvin, G. Gu, E. Nelkin, K. Bowman, Y. Hong, E. Stocker, and D. Wolff (2007), The TRMM multisatellite precipitation analysis: Quasi-global, multi-year, combined sensor precipitation estimates at fine scale, *J. Hydrometeorol., 8*, 38–55.

Intergovernmental Panel on Climate Change (IPCC) (2007), *Climate Change 2007: The Physical Science Basis. Contribution of Working*

Group I to the Fourth Assessment Report of the Intergovernmental Panel on Climate Change, edited by S. Solomon et al., Cambridge Univ. Press, Cambridge, U. K.

Iverson, R. M. (2000), Landslide triggering by rain infiltration, *Water Resour. Res.*, 36, 1897–1910.

Keefer, D., R. Wilson, R. Mark, E. Brabb, W. Brown III, S. Ellen, E. Harp, G. Wieczorek, C. Alger, and R. Zatkin (1987), Real-time landslide warning during heavy rainfall, *Science*, 238, 921–925.

Lawrence, D., and A. Slater (2008), Incorporating organic soil into a global climate model, *Clim. Dyn.*, 30, 145–160.

Potter, C., J. Randerson, C. Field, P. Matson, P. Vitousek, H. Mooney, and S. Klooster (1993), Terrestrial ecosystem production: A process model based on global satellite and surface data, *Global Biogeochem. Cycles.*, 7, 811–841.

Ren, D., and M. Xue (2004), An improved force-restore model for land-surface modeling, *J. Appl. Meteorol.*, 43, 1768–1782.

Ren, D., M. Xue, and A. Henderson-Sellers (2004), The effects of hydraulic lift in simulating superficial soil moisture for vegetated surfaces under dry conditions, *J. Hydrometeorol.*, 5, 1181–1191.

Ren, D., L. M. Leslie, and D. J. Karoly (2007), Sensitivity of an ecological model to soil moisture simulations from two different hydrological models, *Meteorol. Atmos. Phys.*, 100, 87–99.

Ren, D., L. M. Leslie, and D. Karoly (2008), Mudslide risk analysis using a new constitutive relationship for granular flow, *Earth Interact.*, 12, 1–16.

Ye, D., and Y. Gao (1979), *The Tibetan Plateau Meteorology*, Science, Beijing.

Zhang, X., and S. Kondragunta (2006), Estimating forest biomass in the USA using generalized allometric models and MODIS land products, *Geophys. Res. Lett.*, 33, L09402, doi:10.1029/2006GL025879.

———————————

C. Fu and G. Huang, Institute of Atmospheric Physics, Chinese Academy of Sciences, Beijing 100029, China.

R. Fu and D. Ren, Department of Geological Sciences, Jackson School of Geosciences, University of Texas at Austin, 1 University Station C1100, Austin, TX 78712, USA. (diandongren1972@mail.utexas.edu)

Y. Hong, School of Civil Engineering and Environmental Sciences, University of Oklahoma, 202 W. Boyd Street, Norman, OK 73019, USA.

D. J. Karoly, School of Earth Sciences, University of Melbourne, 100 E. Boyd Street, Melbourne, Vic 3010, Australia.

L. M. Leslie, School of Meteorology, University of Oklahoma, 100 East Boyd Street, Norman, OK 73019, USA.

J. Wang, State Key Laboratory of Hydrology-Water Resources and Hydraulic Engineering, Hohai University, Xikang Road 1, Nanjing 210098, China.